Science and Technology of Welding and Joining

ISSN: 1362-1718 (Print) 1743-2936 (Online) Journal homepage: https://www.tandfonline.com/loi/ystw20

Simulations in multipass welds using low transformation temperature filler material

L. Novotný, H. F. G. de Abreu, H. C. de Miranda & M. Béreš

To cite this article: L. Novotný, H. F. G. de Abreu, H. C. de Miranda & M. Béreš (2016) Simulations in multipass welds using low transformation temperature filler material, Science and Technology of Welding and Joining, 21:8, 680-687, DOI: 10.1080/13621718.2016.1177989

To link to this article: https://doi.org/10.1080/13621718.2016.1177989

Published online: 11 May 2016.

Simulations in multipass welds using low transformation temperature filler material

L. Novotný*[1], H. F. G. de Abreu[2], H. C. de Miranda[2] and M. Béreš[2]

Transient thermal and residual stress fields in flux-cored arc welds were examined using a finite element (FE) model. Experimental multipass welds were produced using both conventional and low transformation temperature (LTT) filler metals. Temperature-dependent material properties and both convective and radiant heat loss boundary condition have been considered in the FE model. The effects of the transformation temperature and interpass intervals on residual stresses were examined. It was found that compressive longitudinal residual stresses were developed at the weld centreline in the LTT filler metal. A short-time interpass interval causes the weld fusion zone to be above the martensite start temperature allowing the optimal use of the phase transformation effect. The FE model is sensitive to alteration in welding parameters and can satisfactorily predict the residual stress distribution in welded parts.

Keywords: Welding simulation, Finite element method, Phase transformation, Low transformation temperature filler material, Martensite, Residual stress

Introduction

Although welding is an established industrial practice for metal joining for more than a hundred years, the process is still not fully understood. This is because of the complex nature of the welding process in addition to the absence of appropriate numerical models that take in account all process and physical parameters. Regions in the vicinity of the welding are heated up to the melting temperature of the material and then cooled down by conduction and radiation. Such thermal cycle leads to a non-uniform temperature distribution in the welded components which give rise to large thermal stress gradients causing residual stress and distortion. Furthermore, the individual phases in the material have different physical, thermal and mechanical properties (e.g. thermal expansion, thermal conductivity and yield stress) inducing additional heterogeneity.[1] Therefore, an accurate numerical model should account for temperature-dependent materials properties, phase transformation kinetics, a precise description of the moving heat source, microstructural changes during welding in addition to thermal and transformation strains. The finite element method (FEM) is typically employed to solve the transient thermal fields around the weld. FEM is based on the theory described by Goldak and Akhlaghi.[2] Although finite element (FE) models are simplified in some way, they should keep all the attributes and characteristics necessary for the given approximation level.[3] In many cases, FEM approach was employed considering thermal strains only.[3] However, the austenite to martensite transformation is accompanied by an approximately 5% increase in volume, in addition to volumetric expansion which it is essential to consider.[4] In the present work, both the thermal analysis and resulting stress distribution considering thermal and transformation strains in an experimental weld were performed using FEM approach. The simulations are based on a real welding process of multipass welds produced using low transformation temperature (LTT) filler material.[5] This kind of welding consumable was thoroughly analysed in Refs.[6–16]

Thermal analysis in welding

Mathematical modelling of welding phenomena is very complex and involves solidification phenomena, microstructural changes in the heat-affected zone, heat flux, radiation and thermal stress simulation.[17,18] Calculation consists of thermal and stress analysis and may be coupled or uncoupled.[19] In general, the thermal analysis is assumed to be transient while the stress analysis (elastic–plastic) is quasi static. In most cases, a thermal analysis is first performed to solve temperature fields in the welded component and then results are used as input data for a stress analysis.[20] In solid having uniform material properties (isotropic body), the heat flow in x, y, z directions is proportional to temperature gradient, by Fourier's law

$$q_x = -k\frac{\partial T}{\partial x}, \qquad q_y = -k\frac{\partial T}{\partial y}, \qquad q_z = -k\frac{\partial T}{\partial z} \quad (1)$$

where k is the thermal conductivity (J (m^2 °C s)$^{-1}$), T is the temperature (°C). Magnitudes of q_x, q_y, q_z (J m^{-2}s^{-1}) give the rate of heat flow across a unit area by conduction in subsequent directions. Heat flow is vector and can be

[1]Department of Applied Mechanics and Mechanical Engineering, Technical University of Košice, Letná 9, Košice 04001, Slovak Republic
[2]Department of Metallurgical and Materials Engineering, Federal University of Ceará, Fortaleza, CE, Brazil

*Corresponding author, email ladislav.novotny@gmail.com

Published by Taylor & Francis on behalf of the Institute
Received 12 February 2016; accepted 9 April 2016
DOI 10.1080/13621718.2016.1177989

written in the form

$$\mathbf{q} = \mathbf{i}q_x + \mathbf{j}q_y + \mathbf{k}q_z.$$

Then equation (1) can be written in vector form

$$\mathbf{q} = -k\nabla T,$$

where ∇ is the nabla (Hamilton) operator

$$\nabla = \mathbf{i}\frac{\partial}{\partial x} + \mathbf{j}\frac{\partial}{\partial y} + \mathbf{k}\frac{\partial}{\partial z}$$

The energy balance equation for transient heat conduction analysis is given by the formula

$$k\left(\frac{\partial^2 T}{\partial x^2} + \frac{\partial^2 T}{\partial y^2} + \frac{\partial^2 T}{\partial z^2}\right) + g = \rho c_p \frac{\partial T}{\partial t}, \quad (2)$$

where t is the time (s), ρ is the density (kg m^{-3}), c_p is the specific-heat capacity (J kg^{-1} °C^{-1}), g is the rate of heat generated per unit volume and per unit time (J m^{-3} s^{-1}). This equation can be written in the form

$$k\Delta T + g = \rho c_p \frac{\partial T}{\partial t}, \quad (3)$$

where Δ is the Laplace operator given by formula

$$\Delta = \nabla \cdot \nabla = \nabla^2 = \frac{\partial^2}{\partial x^2} + \frac{\partial^2}{\partial y^2} + \frac{\partial^2}{\partial z^2}.$$

Initial and boundary conditions are needed to be prescribed to solve equation (2). In transient heat transfer problems, the temperature field in the material changes with time, initial temperature is

$$T(\mathbf{x}, t = 0) = T_0(x, y, z).$$

Common boundary conditions in transient analysis are temperature, surface heat flux, volumetric heat flux, convection and radiation. Temperature prescribed on the region Γ_T in time t (Dirichlet boundary condition) is written as

$$T(\mathbf{x}, t) = T_d(x, y, z, t), \mathbf{x} \in \Gamma_T.$$

Surface heat flux $q^*(x, y, z, t)$ for the surface region Γ_q (Neumann boundary condition) is written as

$$-\mathbf{q}(\mathbf{x}, t) \cdot \mathbf{n} = -q(\mathbf{x}, t) = q^*(x, y, z, t), \mathbf{x} \in \Gamma_q,$$

where $\mathbf{n}$ is the unit vector of external normal line on Γ_q region. Surface heat flux is positive value if heat gets inside to region. Volumetric heat flux $r^*(x, y, z, t)$ for the surface region Γ_r is written as

$$-g(\mathbf{x}, t) = r(\mathbf{x}, t) = r^*(x, y, z, t), \mathbf{x} \in \Gamma_r.$$

Convection $q_c^*(x, y, z, t)$ defined on surface region Γ_c is calculated by

$$\begin{aligned}\mathbf{q}(\mathbf{x}, t) \cdot \mathbf{n} &= q_c(\mathbf{x}, t) = q_c^*(x, y, z, t) \\ &= h \cdot (T - T_b), \mathbf{x} \in \Gamma_c, \end{aligned} \quad (4)$$

where h is the film coefficient (J (m^2 °C s)$^{-1}$), T is the temperature on the surface region Γ_c and T_b is the sink temperature (°C).

Radiation $q_r^*(x, y, z, t)$ defined on the surface region Γ_r is calculated by

$$\begin{aligned}\mathbf{q}(\mathbf{x}, t) \cdot \mathbf{n} &= q_r(\mathbf{x}, t) = q_r^*(x, y, z, t) \\ &= A \cdot ((T - 273^\circ\text{C})^4 - (T_b - 273^\circ\text{C})^4) \\ &= \varepsilon \cdot \sigma \cdot ((T - 273^\circ\text{C})^4 - (T_b - 273^\circ\text{C})^4), \mathbf{x} \in \Gamma_r,\end{aligned}$$

where A is the radiation constant (J (m^2 K^4 s)$^{-1}$), σ is the Stefan–Boltzmann constant ($\sigma \doteq 5,67 \times 10^{-8}$ J m^{-2} K^{-4} s^{-1}), ε is the emissivity $0 < \varepsilon < 1$ ($\varepsilon = 1$ for ideal radiant-black body), T (°C) is the temperature on the surface region, Γ_c, T_b is the sink temperature (°C).

Moving heat sources

During welding, the heat energy is supplied to the solidus area. In arc welding, the heat input can be expressed by

$$\dot{Q} = UI\eta,$$

where Q (J) is the available heat ($\dot{Q}$ is input heat per time (W)), I is the current (A), U is the voltage (V) between the electrode and baseplate, η is efficiency of heat input, which takes into account loss of energy by radiation and convection. High efficiency such as $\eta = 0.9 - 0.99$ is expected in submerged arc welding, low efficiency $\eta = 0.3 - 0.6$ in tungsten inert gas (TIG) welding. Distribution of heat flow is not constant along directions and also depends on each welding process.[21,22]

Goldak proposed double ellipsoid model for modelling of heat source.[2] The model uses Gaussian distribution of heat input and is practical for modelling of heat source in simulation of TIG, MIG (metal inert gas) or flux-cored arc welding (FCAW) process. Moving heat source can be also defined by convection $q_c^*(x, y, z, t)$ (equation (4)) on the surface region Γ_c which is equal to position of weld torch (moving in z direction), and with the sink temperature T_b (°C) which is equal to melt temperature T_m (°C)

$$q_c^*(x, z, t) = h \cdot (T - T_b) = h \cdot (T - T_m).$$

Experimental welds, numerical calculations

Below, an example of welding simulation based on experimental multipass welds[5] is presented. Experimental trials were performed at the Department of Metallurgical and Materials Engineering, Federal University of Ceará, Fortaleza/Brazil. Sections of pipeline, with dimensions presented in Fig. 1*a*, were welded in five passes employing FCAW automatic process.

Both, a conventional and a LTT, weld filler materials were used. The chemical composition of both filler materials and that of the base metal is shown in Table 1. Solid state austenite to martensite/ferrite transformation start temperature in the conventional and LTT filer material were 560 and 180°C, respectively. Welding conditions for the conventional weld filler material were – voltage $U_c = 24$ V, current $A_c = 210$ A. For the LTT weld filler material, following parameters were employed – voltage $U_{LTT} = 28$ V, current $v_C = v_{LTT} = 5$ mm s^{-1}. The welding wire speed for

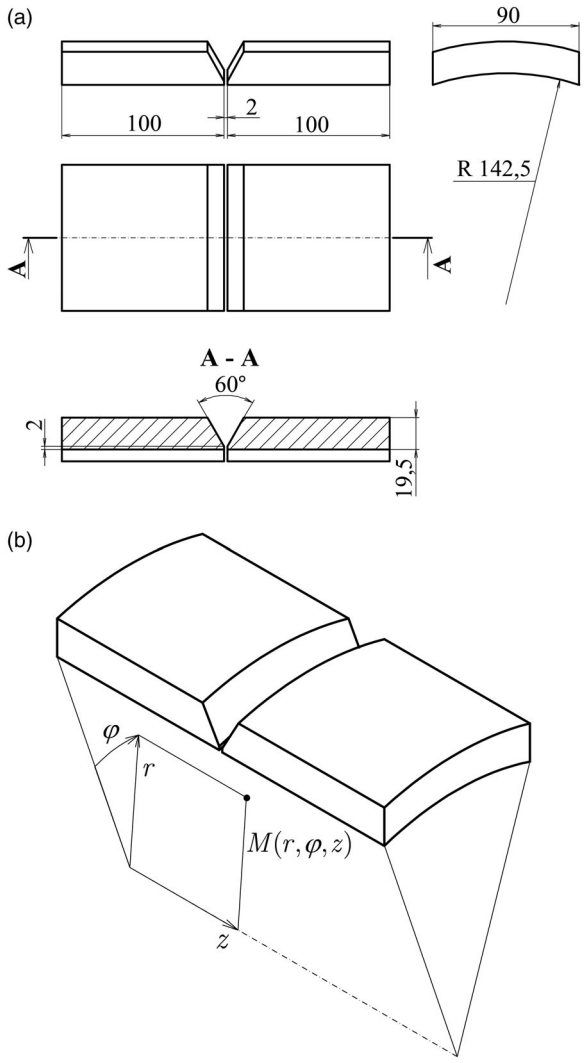

1 ***a*** **Schematic representation of the welded sample,** ***b*** **definition of cylindrical coordinate system**

both weld consumables was maintained at $v_C = v_{LTT} = 5\,\text{mm}\,\text{s}^{-1}$, joint preparation angle was 60°, root gap was 2 mm (Fig. 1*a*).

A K-type thermocouple, located on the bottom side at the mid-length of the sample 4 mm away from the centreline, was used to monitor the temperature changes during welding.

The residual stress was measured by the X-ray diffraction using chromium K_α radiation. The operating voltage and current were 20 kV and 50 mA, respectively. The $\sin^2\psi$ technique was used with ψ angle variation between −45 and +45°. Before the measurements, surfaces perpendicular to the weld seam in the mid-length of the sample were etched using ammonium chloride (NH_4Cl) electrolyte. At these etched surfaces, 15 points 3 mm apart from each other (distance −18 mm and +18 mm from centreline with first measurement point being at weld centreline), were selected to perform residual stress measurements.

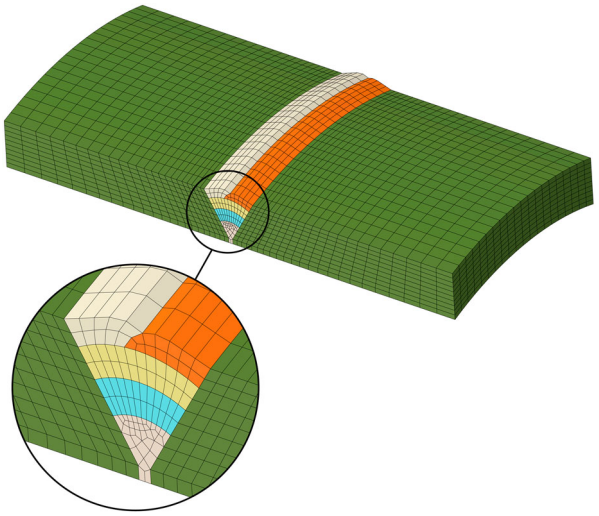

2 Finite element model of weld sample showing weld seams

At each point, stresses along the weld seam-longitudinal residual stresses and perpendicular to the weld seam-transverse residual stresses were measured (the longitudinal and transverse directions are explained in details in the section 'Results and discussion'). Further experimental details can be found in Abreu *et al.*[5]

An FE model of the weld with highlighted weld beads is presented in Fig. 2. The contour of each bead approximately corresponds to the actual weld seam shape observed in macrograph of the welded joint.[5] Interpass intervals were 420, 450, 700 and 530 s equally as in experiment.

During welding of ferritic steel, if phase transformation occurs, latent heat and transformation strain is generated. In the solution of equation (2), the latent heat was included by using an equivalent specific-heat capacity c_p^e.[23] The components of the total strain rate $\dot{\varepsilon}_{ij}$ can be decomposed into the sum of elastic strain rate components $\dot{\varepsilon}_{ij}^e$, plastic strain rate components $\dot{\varepsilon}_{ij}^p$, thermal strain rate components $\dot{\varepsilon}_{ij}^{th}$, transformation strain rate components $\dot{\varepsilon}_{ij}^{tr}$

$$\dot{\varepsilon}_{ij} = \dot{\varepsilon}_{ij}^e + \dot{\varepsilon}_{ij}^p + \dot{\varepsilon}_{ij}^{th} + \dot{\varepsilon}_{ij}^{tr}. \quad (5)$$

Elastic strain rate components $\dot{\varepsilon}_{ij}^e$ can be written in the form

$$\dot{\varepsilon}_{ij}^e = C_{ijkl}(T)\dot{\sigma}_{kl},$$

where $C_{ijkl}(T)$ are components of the second-order compliance tensor, σ_{ij} are components of the stress tensor. Plastic strain rate components $\dot{\varepsilon}_{ij}^p$ are most commonly expressed in the form

$$\dot{\varepsilon}_{ij}^p = \dot{\lambda}\frac{\partial\psi}{\partial\sigma_{ij}},$$

where ψ is the scalar function and represents the plastic potential, $\dot{\lambda}$ is the scalar parameter (scalar multiplier).

Table 1 Chemical composition (wt-%) of base metal and weld filler materials

	C	Mn	Si	Cr	Ni	Mo	N	Al
Base metal (API 5L Grade B PSL1)	0.13	0.89	0.12	0.03	0.01	0.03	…	…
Conventional weld filler (ESAB OK TUBROD 711 OA)	0.25	0.7	0.4	…	…	…	…	1.6
LTT weld filler	0.08	1	0.6	13.5	4.3	0.5	0.1	…

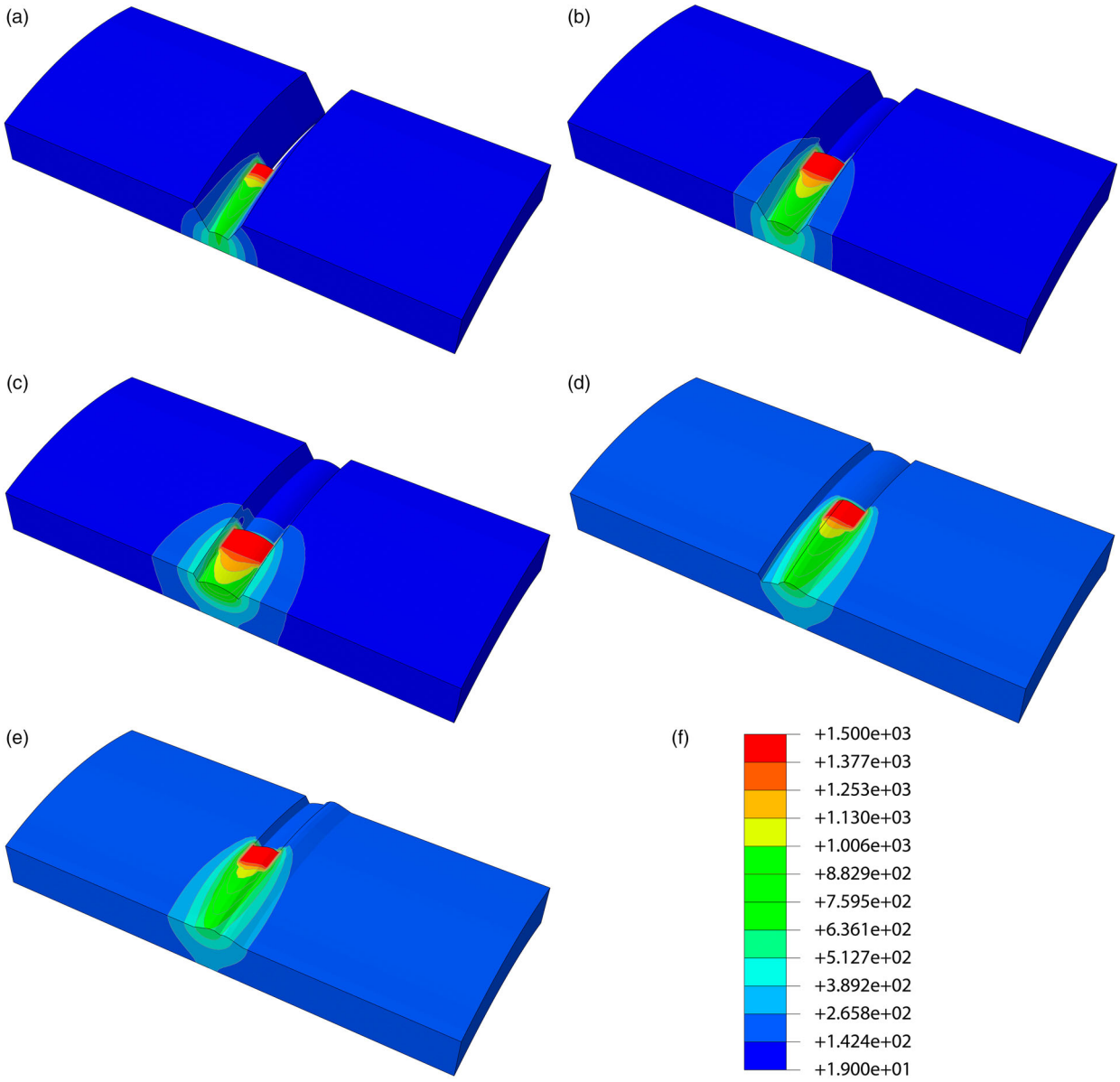

3 Predicted temperature distribution in the welded component *T* (°C) using conventional filler material for *a* the first pass in time 7.5 s, *b* the second pass in time 447 s, *c* the third pass in time 914 s, *d* the fourth pass in time 1640 s, *e* the fifth pass in time 2190 s, *f* colour legend indicates temperature *T* (°C)

Thermal strain rate components $\dot{\varepsilon}_{ij}^{\text{th}}$ can be calculated by formula

$$\dot{\varepsilon}_{ij}^{\text{th}} = \alpha(T)\dot{T}\delta_{ij}, \tag{6}$$

where $\alpha(T)$ is the thermal expansion coefficient (°C^{-1}). The steel microstructure can be composed of various phases (austenite, ferrite, perlite, bainite, martensite, cementite). In regard of their phase fraction, the following must be valid

$$\sum_{i=1}^{n} P_i(T, t) = 1,$$

where $P_i(T, t)$ is the phase fraction of i phase. If Ω_{ij} is defined as phase fraction i originated from phase j, then

$$\dot{P}_i = \sum_{i=1}^{n} \dot{\Omega}_{ij}.$$

Transformation strain rate components $\dot{\varepsilon}_{ij}^{\text{tr}}$ can be calculated from equation

$$\dot{\varepsilon}_{ij}^{\text{tr}} = \bar{\varepsilon}_{kl}^{\text{tr}}\dot{\Omega}_{kl}\delta_{ij}, \tag{8}$$

where $\bar{\varepsilon}_{kl}^{\text{tr}}$ is the material constant and represents the strain corresponding to a fully transformed phase l to phase k.[23] The martensitic transformation is diffusionless and takes place only in non-isothermal processes.[24] The formation of martensite during cooling begins at temperature M_{s} and finishes at temperature M_{f}. The volume fraction of martensitic transformation can be computed by using Koistinen–Marburger law

$$P(T) = P_{\text{A}}(1 - e^{-k(M_{\text{s}}-T)}), \tag{9}$$

where P_{A} is the residual volume fraction of austenite at temperature M_{s}, k is the constant and can be determined

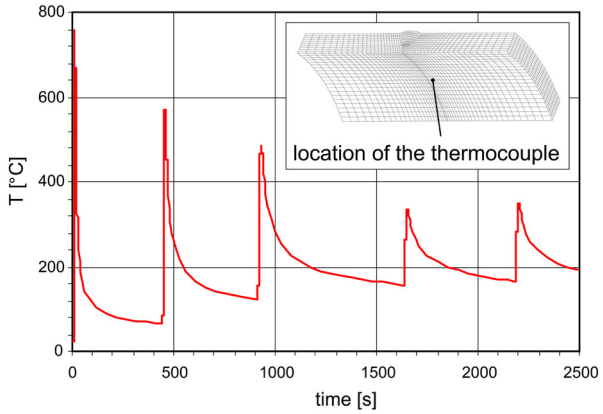

4 Calculated thermal cycle *T* (°C) at the location of thermocouple (conventional filler material)

experimentally.[25] In equation (9), $P(T)$ depends only on the temperature T, so if only martensitic transformation occurs, then $\dot{\Omega}_{kl}$ depends only on the temperature T too, equation (8), considering equation (7), can be written in the form

$$\dot{\varepsilon}_{ij}^{\mathrm{trM}} = \bar{\varepsilon}_{kl}^{\mathrm{tr}}\dot{\Omega}_{kl}(T)\delta_{ij} = \bar{\varepsilon}_{\mathrm{M}}^{\mathrm{tr}}\dot{P}\delta_{ij} = \bar{\varepsilon}_{\mathrm{M}}^{\mathrm{tr}}(-P_A)ke^{-k(M_s-T)}\dot{T}\delta_{ij}. \quad (10)$$

Thermal strain rate components $\dot{\varepsilon}_{ij}^{\mathrm{th}}$ and transformation strain rate components $\dot{\varepsilon}_{ij}^{\mathrm{tr}}$ can be calculated together, considering that equations (10) and (6) have a similar form

$$\dot{\varepsilon}_{ij}^{\mathrm{th}} + \dot{\varepsilon}_{ij}^{\mathrm{tr}} = \alpha(T)\dot{T}\delta_{ij} + \bar{\varepsilon}_{\mathrm{M}}^{\mathrm{tr}}(-k)P_{\mathrm{A}}e^{-k(M_s-T)}\dot{T}\delta_{ij} = [\alpha(T) + \bar{\varepsilon}_{\mathrm{M}}^{\mathrm{tr}}(-k)P_{\mathrm{A}}e^{-k(M_s-T)}]\dot{T}\delta_{ij}. \quad (11)$$

Numerical calculations consisted of thermal and stress analysis and were considered as uncoupled (temperature fields were independent of the stress fields and strain fields). The thermal analysis was considered as transient, the stress analysis was considered as quasi static (no inertia forces were considered), the elastic–plastic material law was considered. The temperature-dependent material thermo-physical and mechanical properties for individual materials (LTT filler material[26] and conventional filler material,[26] base material[27]) were incorporated in the numerical model. Transformation strain rate components $\dot{\varepsilon}_{ij}^{\mathrm{tr}}$ in case of the martensitic transformation were included based on equation (8) considering $\bar{\varepsilon}^{\mathrm{trM}} = 9.9 \times 10^{-3}$.[28] The element birth technique was used in the calculation.

Results and discussion

The results of thermal analysis with transient temperature fields during the weld pass of appropriate beads (conventional filler material) are shown in Fig. 3. The heat flow

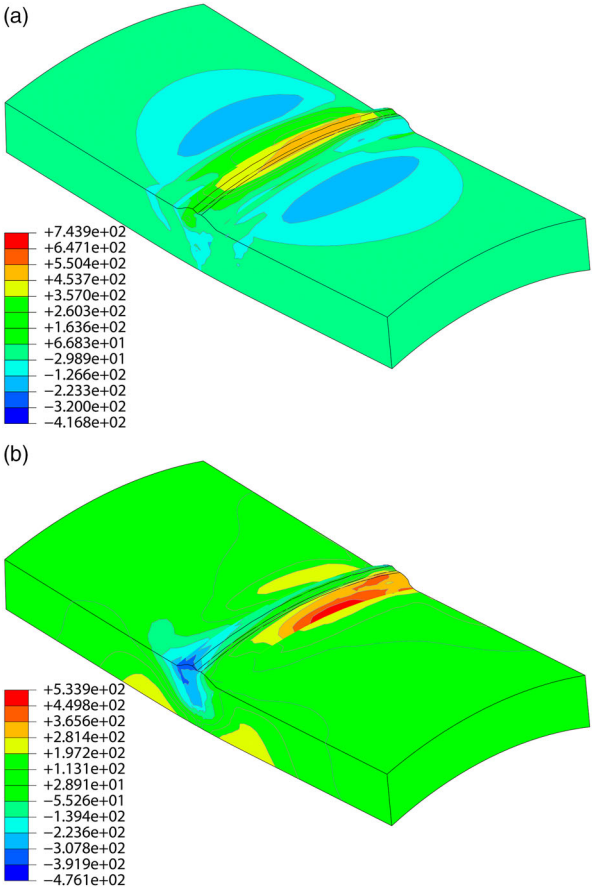

5 Predicted residual stress (MPa) distribution in *a* longitudinal and *b* transverse direction (cylindrical coordinate system), conventional filler material

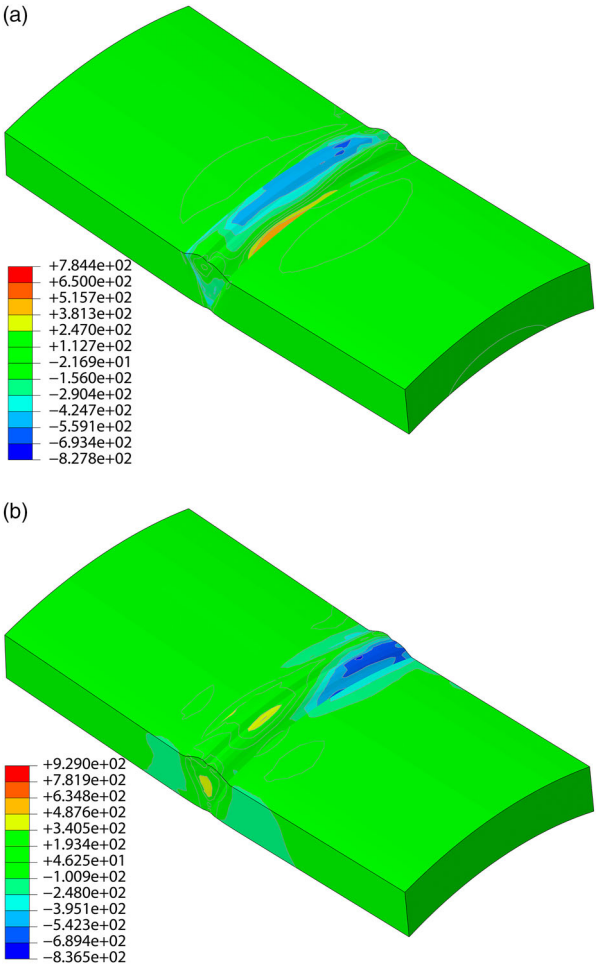

6 Predicted residual stress (MPa) distribution in *a* longitudinal and *b* transverse direction (cylindrical coordinate system), LTT filler material

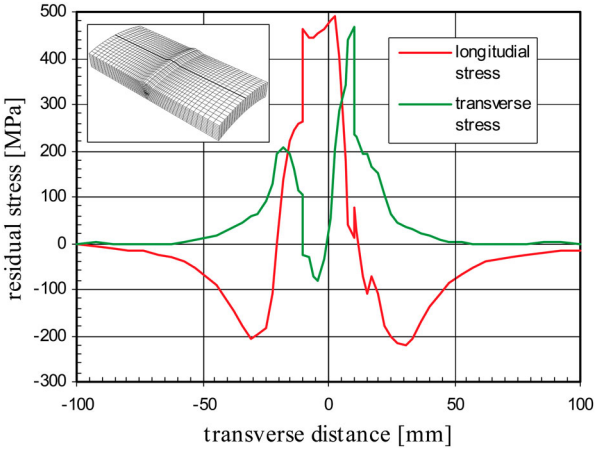

7 Predicted longitudinal and transverse residual stress distribution at the curve in the mid-length of the sample (cylindrical coordinate system), conventional filler material

from weld beads to the weld plate can be also seen in these fields. The calculated thermal cycle at the location of the thermocouple is presented in Fig. 4; the position of thermocouple on the bottom side 4 mm away from the centreline is also shown.

The normal component of the stress tensor in the tangential direction is called longitudinal stress, σ_φ, the normal component of the stress tensor in z direction (Fig. 1*b*) is called transverse stress, σ_z. The residual stress fields calculated for the conventional filler material are shown in Fig. 5; the residual stress fields calculated for the LTT filler material are shown in Fig. 6. Components of the stress tensor (Figs. 5 and 6) are represented in the cylindrical coordinate system which is defined in Fig. 1*b*.

The longitudinal residual stress σ_φ and transverse residual stress σ_z distribution calculated for the conventional filler material is shown in Fig. 7 (along the perpendicular curve to the weld line). The longitudinal residual stress σ_φ and transverse residual stress σ_z calculated for the LTT filler material is shown in Fig. 8 (along the perpendicular curve to the weld line).

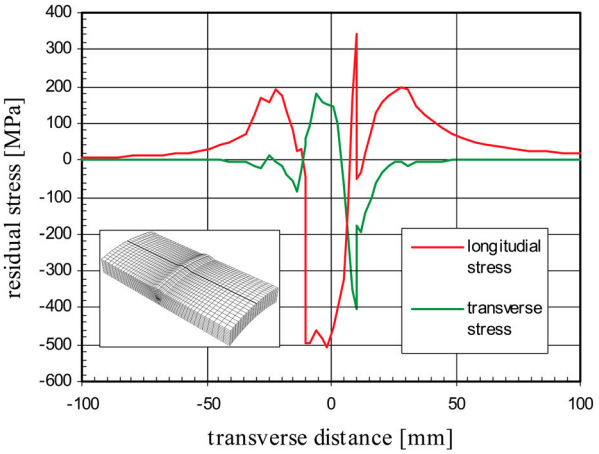

8 Predicted longitudinal and transverse residual stress distribution at the curve in the mid-length of the sample (cylindrical coordinate system), LTT filler material

In conventional weld filler, the longitudinal stresses in the weld region are of a positive value (tensile stresses) and around the weld have a negative value (compressive stresses), Fig. 7. The residual stress in the transversal direction is negative (compressive stresses) and heterogeneously distributed through thickness (Figs. 5*b* and 7) causing an undesirable transverse deformation.

The research of Murakawa *et al.*[26] showed that using LTT filler material, the volumetric expansion of the material during phase transformation austenite to martensite, i.e. the transformation strains $\dot{\varepsilon}_{ij}^{\mathrm{tr}}$ (defined in equations (6) and (9)) is positive during the cooling. This volumetric expansion, causes longitudinal stresses in the weld regions, will be negative (compressive stresses), Fig. 8. The compressive stresses are preferable for cyclic loading and for fatigue strength improvement as shown by Ohta *et al.*[29] In addition, the use of LTT weld filler material causes positive transverse stresses to be generated through thickness as shown in Fig. 6*b* which leads to reduction in distortion.

Both the simulation and experimental results confirmed the above-mentioned facts about the use of the LTT weld wire material. Similar values of residual stresses using LTT weld wire material can be found in the work of Ramjaun *et al.*[30]

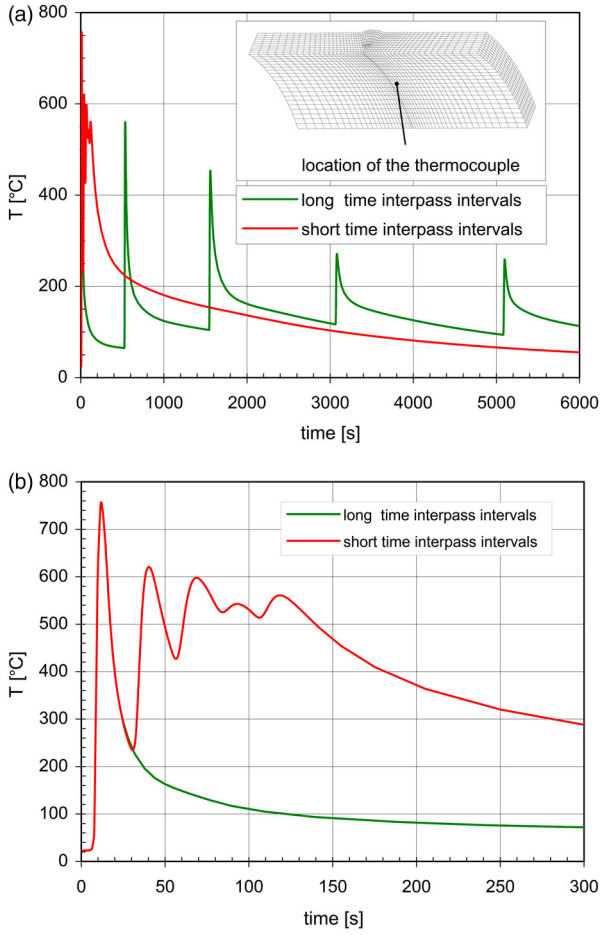

9 *a* Calculated thermal cycle *T* (°C) at the location of thermocouple (LTT filler material) for both short- and long-time interpass intervals, *b* thermal cycle in detail

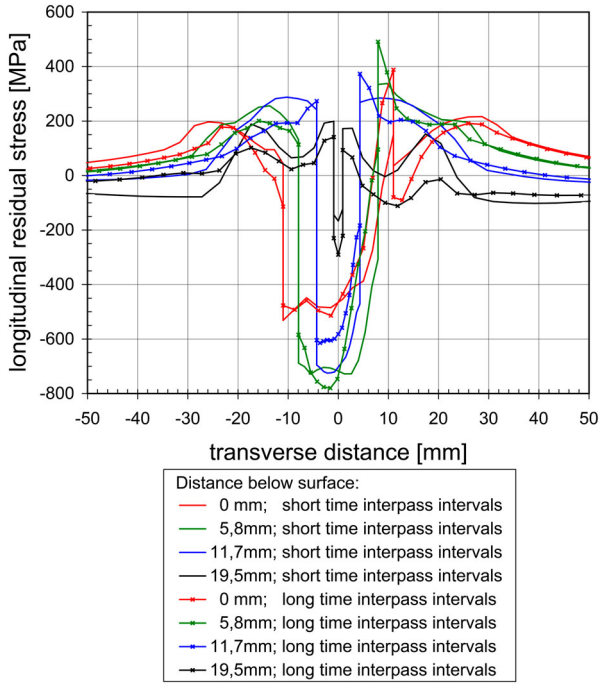

10 Predicted longitudinal residual stress distribution in the LTT filler material for both short- and long-time interpass intervals as function of distance from weld centreline, cylindrical coordinate system

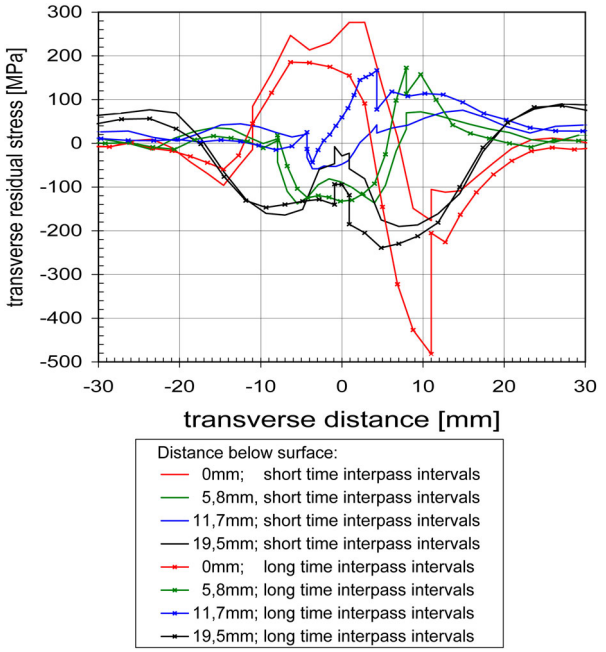

11 Predicted transverse residual stress distribution in the LTT filler material for both short- and long-time interpass intervals as function of distance from weld centreline, cylindrical coordinate system

Sensitivity study of FE model to alteration in welding parameters

In this section, sensitivity of proposed FEM to alteration in welding parameters, i.e. time interval between each deposited layer using LTT filler material is demonstrated. First case considered long-time interpass intervals, i.e. 500, 1000, 1500, 2000 and 10 000 s enabling each individual welding pass is fully transformed to martensite before the next layer is deposited. Computed thermal cycle for this case is shown in Fig. 9*a* (green line). One can see that the weld region cools down below M_s temperature, i.e. 180°C after each deposited layer. Second case assumed short-time intervals between each deposited layer, i.e. 5 s, permitting the interpass temperature to be maintained above M_s for all passes. The welded sample was finally allowed to cool to room temperature. A detailed view of thermal history for short-time interpass intervals, red line in Fig. 9*b*, revealed that the interpass temperature for all deposited layers was maintained in excess of M_s. This causes that layers 1–5 transform collectively into martensite after 5th pass is completed allowing optimal use of phase transformation effect.

Figure 10 shows computed longitudinal residual stress profiles in the LTT filler material for both long- and short-time interpass intervals. Stress analysis was performed across a plane perpendicular to the weld seam in the mid-length of the sample, as shown in Figs. 7 and 8, at surface in addition to 5.8 mm, 11.7 mm and 19.5 mm below surface. At surface, compressive residual stresses of ~500 MPa were generated, whereas stresses of ~200 MPa were found at 19.5 mm below surface. Largest residual stresses of ~800 MPa were induced at a depth of 5.8 mm below surface during long-time interpass intervals. In comparison to short-time interpass intervals, these stresses are higher in magnitude, however, cover smaller field. Thus, the phase transformation effect can be fully exploited if the whole multipass weld metal transforms at once after last layer has been deposited. Similar results were observed in Ramjaun *et al.*[30]

Predicted transverse residual stress profiles in the LTT filler material for short- and long-time interpass intervals are shown in Fig. 11. Tensile transverse residual stresses of ~200 MPa were generated at the surface, whereas compressive transverse residual stresses of ~130 MPa were found at 5.8 and 19.5 mm below surface. Short-time interpass intervals cause a shift towards positive stresses at the surface and in the root pass. Transverse residual stresses in the mid-thickness increased during long-time interpass intervals.

Conclusions

A three-dimensional FE model was developed to analyse temperature fields and residual stresses during multipass FCAW process employing both conventional and LTT weld filler materials.

The numerical and experimental results indicate that use of weld metals with different transformation characteristics has substantial impact on residual stress patterns. The LTT welding alloy induced compressive longitudinal residual stresses in the weld zone and its vicinity. This was in contrast to the conventional weld filler where tensile longitudinal residual stresses were found. Transformation plasticity is fully exploited if the interpass temperature is maintained above M_s for all passes and the entire weld metal transforms during cooling after the last layer has been deposited. The proposed analytical model is sensitive to alteration in welding parameters and can satisfactorily predict the residual stress distribution in welded parts.

Funding

This work was supported by the Scientific Grant Agency of Ministry of Education, Science, Research and Sport of the Slovak Republic (grant number VEGA 2/0098/14).

References

1. H. K. D. H. Bhadeshia: 'Bainite in steels', 2nd edn, Vol. 1, 240–249; 2001, London, Maney.
2. J. A. Goldak and M. Akhlaghi: 'Computational welding mechanics', 2005, London, Springer.
3. L. Novotný and M. Tsunori: 'Creation of imperfections for welding simulations', *Comput. Model. Eng. Sci.*, 2011, **82**, (3&4), 253–264.
4. T. Alghamdi and S. Liu: 'Low-transformation-temperature (LTT) welding consumables development and testing qualification', *Weld. J.*, 2014, **93**, 243–252.
5. H. F. G. Abreu, W. S. Tavares, H. C. Miranda, M. P. C. Foncesa, H. N. Virgens-Neto and M. Béreš: 'Effect of multipass welding using a low transformation temperature filler metal on residual stress and toughness', *Mater. Sci. Forum*, 2014, **783–786**, 627–632.
6. J. Eckerlid, T. Nilsson and L. Karlsson: 'Fatigue properties of longitudinal attach-ments welded using low transformation temperature filler', *Sci. Technol. Weld. Join.*, 2003, **8**, 353–359.
7. J. Yamamoto, K. Hiraoka and M. Mochizuki: 'Analysis of martensite transformation behaviour in welded joint using low transformation temperature welding wire', *Sci. Technol. Weld. Join.*, 2010, **15**, (2), 104–110.
8. L. Y. Xu, Y. F. Wang, H. Y. Jing and Y. D. Han: 'Fatigue strength improvement of stainless steel using weld toes dressing with low transformation temperature welding wire', *Sci. Technol. Weld. Join.*, 2014, **19**, (8), 664–672.
9. M. Béreš, H. F. G. Abreu, L. P. M. Santos, C. M. Davies and D. Dye: 'Effect of variant transformations in fusion zones of gas metal arc welds', *Sci. Technol. Weld. Join.*, 2015, **20**, (4), 353–360.
10. M. C. Payares-Asprino, H. Katsumoto and S. Liu: 'Effect of martensite start and finish temperature on residual stress development in structural steel welds', *Weld. J.*, 2008, **87**, 279–289.
11. R. J. Moat, H. J. Stone, A. A. Shirzadi, J. A. Francis, S. Kundu, A. F. Mark, H. K. D. H. Bhadeshia, L. Karlsson and P. J. Withers: 'Design of weld fillers for mitigation of residual stresses in ferritic and austenitic steel welds', *Sci. Technol. Weld. Join.*, 2011, **16**, 279–284.
12. S. H. Thomas and S. Liu: 'Analysis of low transformation temperature welding (LTTW) consumables–distortion control and evolution of stresses', *Sci. Technol. Weld. Join.*, 2007, **12**, (6), 516–522.
13. S. Zenitani, N. Hayakawa, J. Yamamoto, K. Hiraoka, Y. Morikage, T. Kubo, K. Yasuda and K. Amano: 'Development of new low transformation temperature welding consumable to prevent cold cracking in high strength steel welds', *Sci. Technol. Weld. Join.*, 2014, **19**, (5), 392–401.
14. T. I. Ramjaun, H. J. Stone, L. Karlsson, J. Kelleher, S. W. Ooi, K. Dalaei, J. Rebelo Kornmeier and H. K. D. H. Bhadeshia: 'Effects of dilution and baseplate strength on stress distributions in multipass welds deposited using low transformation temperature filler alloys', *Sci. Technol. Weld. Join.*, 2014, **19**, (6), 461–467.
15. T. I. Ramjaun, H. J. Stone, L. Karlsson, M. A. Gharghouri, K. Dalaei, R. J. Moat and H. K. D. H. Bhadeshia: 'Surface residual stresses in multipass welds produced using low transformation temperature filler alloys', *Sci. Technol. Weld. Join.*, 2014, **19**, (7), 623–630.
16. Y. Mikami, Y. Morikage, M. Mochizuki and M. Toyoda: 'Angular distortion of fillet welded T joint using low transformation temperature welding wire', *Sci. Technol. Weld. Join.*, 2009, **14**, 97–105.
17. A. A. Shirzadi, H. K. D. H. Bhadeshia, L. Karlsson and P. J. Withers: 'Stainless steel weld metal designed to mitigate residual stresses', *Sci. Technol. Weld. Join.*, 2009, **14**, (6), 559–565.
18. H. Dai, J. A. Francis, H. J. Stone, H. K. D. H. Bhadeshia and P. J. Withers: 'Characterizing phase transformations and their effects on ferritic weld residual stresses with x-rays and neutrons', *Metall. Mater. Trans. A*, 2008, **39**, (13), 3070–3078.
19. L. Ceniga: 'A new analytical model for thermal stresses in multiphase materials and lifetime prediction methods', *Acta Mech. Sinica*, 2008, **24**, 189–206.
20. I. S. Leoveanu, and G. Zgura: 'Modelling the heat and fluid flow in the welded pool from high power arc sources', *Mater. Sci. Forum*, 2008, **580–582**, 443–446.
21. P. Colegrove, C. Ikeagu, A. Thistlethwaite, S. Williams, T. Nagy, W. Suder, A. Steuwer and T. Pirling: 'Welding process impact on residual stress and distortion', *Sci. Technol. Weld. Join.*, 2009, **14**, (8), 717–725.
22. P. Colegrove, H. Shercliff and R. Zettler: 'Model for predicting heat generation and temperature in friction stir welding from the material properties', *Sci. Technol. Weld. Join.*, 2007, **12**, (4), 284–297.
23. L. Novotný and V. Ivančo: 'Calculations of phase transformations in welding simulations', *Appl. Mech. Mater.*, 2014, **611**, 46–53.
24. R. V. Andrade: 'Pipe circularity reformation via line heating', 2001, Cambridge, MA, Massachusetts Institute of Technology.
25. P. Papon, J. Leblond and P. H. E. Meijer: 'The physics of phase transitions–concepts and applications', 2006, Berlin, Springer.
26. H. Murakawa, M. Béreš, C. Davies, S. Rashed, A. Vega, M. Tsunori, K. Nikbin and D. Day: 'The effect of low transformation temperature weld filler metal on welding residual stress', *Sci. Technol. Weld. Join.*, 2010, **15**, (5), 393–399.
27. M. R. Frouzan, S. M. Mirfalah, A. Mokhtari, A. Heidari and S. J. Golestaneh: 'Residual stress prediction in submerged arc welded spiral pipes', *Mater. Des.*, 2012, **33**, 384–394.
28. M. Jung, M. Kang and Y. K. Lee: 'Finite-element simulation of quenching incorporating improved transformation kinetics in a plain medium-carbon steel', *Acta Mater.*, 2012, **60**, 525–536.
29. A. Ohta, O. Watanabe, K. Matsuoka, T. Shiga, S. Nishijima, Y. Maeda, N. Suzuki and T. Kubo: 'Fatigue strength improvement by using newly developed low transformation temperature welding material', *Weld. World*, 1999, **43**, 38–42.
30. T. I. Ramjaun, H. J. Stone, L. Karlsson, J. Kelleher, R. J. Moat, J. R. Kornmeier, K. Dalaei and H. K. D. H. Bhadeshia: 'The effect of interpass temperature on residual stresses in multi-pass welds produced using a low transformation temperature filler alloy', *Sci. Technol. Weld. Join.*, 2014, **19**, 44–51.